Flexural Behaviour of Precast Segmental Concrete Beams Internally Prestressed with Unbonded CFRP Tendons under Four-point Loading

Tan D. Le[1], Thong M. Pham[2], Hong Hao[3] and Yifei Hao[4]

Abstract

This study investigates the use of carbon fibre reinforced polymer (CFRP) tendons on precast segmental beams (PSBs) to tackle the corrosion problems which are likely to occur at joint locations of PSBs prestressed with steel tendons. Up to date, the use of CFRP tendons was extensively documented for monolithic beams while their application on PSBs has not been reported yet. Three precast segmental T-section beams including two beams with unbonded CFRP and one with steel tendons were built and tested under four-point loads in this study. The test results showed that CFRP tendons can be well used to replace the steel tendons on PSBs. The beams with CFRP tendons demonstrated both high strength and high ductility as compared to the beam with steel tendons. However, the stresses in the unbonded CFRP tendons at ultimate loading conditions of the tested beams were low, ranging from only about 66% to 72% of the nominal breaking tensile strength. The type of joints i.e. dry and epoxied, greatly affects the initial stiffness of the beams but has no effect on the opening of joints at ultimate loading stage. Moreover, a comprehensive examination on four existing code equations to predict the stress in the unbonded tendons showed that the four examined codes predicted well

[1]PhD Scholar, Center for Infrastructural Monitoring and Protection, School of Civil and Mechanical Engineering, Curtin University, Kent Street, Bentley, WA 6102, Australia. Email: tan.le1@postgrad.curtin.edu.au
[2]Research Fellow, Center for Infrastructural Monitoring and Protection, School of Civil and Mechanical Engineering, Curtin University, Kent Street, Bentley, WA 6102, Australia, (corresponding author). Email: thong.pham@curtin.edu.au
[3]John Curtin Distinguished Professor, Center for Infrastructural Monitoring and Protection, School of Civil and Mechanical Engineering, Curtin University, Kent Street, Bentley, WA 6102, Australia, and School of Civil Engineering, Guangzhou University, Guangzhou 510006, China, (corresponding author). Email: hong.hao@curtin.edu.au
[4] Professor, Key Laboratory of Coast Civil and Structure Safety of Ministry of Education, Tianjin University, Tianjin, 300072, China. Email: hao.yifei@tju.edu.cn

the stress at the ultimate loading condition of the unbonded steel tendons, however, they significantly under predicted those in the CFRP tendons. A modification in the strain reduction coefficient used by ACI 440.4R for predicting the stress increment in unbonded CFRP tendons of monolithic beams is therefore proposed for PSBs based on the experimental results.

Keywords: segmental concrete beams; fibre reinforced polymer (FRP) tendons; internal unbonded tendons; posttensioning; shear-keyed joints.

1 Introduction

Since its first application for concrete bridges in 1950's, precast segmental prestressed concrete girder bridges have gained rapid acceptance as they not only allow speeding up the construction process but also improving the quality control. So far, steel tendons have been used as the only prestressing solution to connect individual beam segments to form the completed bridge spans. The steel tendons can be bonded or unbonded to the concrete and placed inside or outside of the beam cross-section, known as internally or externally prestressing techniques. Corrosion of steel tendons at joint locations, however, causes deterioration or even total collapse of the whole structures [1-3] .

Fibre reinforced polymer (FRP) tendons have been used for the prestressing technique as a promising solution to replace steel tendons to deal with the corrosion issue. The term "FRP tendons" denotes the use of one of various types of fibres, i.e. aramid (AFRP), carbon (CFRP) or glass (GFRP). In the literature, the use of FRP tendons have only been applied to monolithic concrete beams [4]. When tendons are internally bonded to the concrete, FRP and steel prestressed beams behave differently after concrete cracked [4-6]. In the first stage, both beams with FRP and steel tendons will deform elastically until cracking of concrete. After cracking, beams prestressed with steel tendons exhibits nonlinear load-deflection behaviour until the beams fail by crushing of concrete or rupture of tendons. In contrast, beams prestressed with FRP tendons will continue to deform in an approximately linear manner with the increase in the applied load until the tendons rupture or the concrete reaches its ultimate compressive strain. Furthermore, Maissen and de Smet [6] reported that the moment redistribution mechanism in the beams prestressed with CFRP tendons differed from that of the beams with steel tendons because CFRP tendons did not exhibit elasto-plastic deformation characteristics. Zou [7] pointed out that the conventional ductility index for concrete beams prestressed with steel tendons was not suitable for beams with FRP tendons since FRP did not have a yield point. As such, a new deformability index counting for both deflection and strength factors was proposed and it applied to beams with either FRP tendons or steel tendons. It is noted that this proposed deformability index was based on the analysis of monolithic beams prestressed with carbon fibre reinforced polymer (CFRP) tendons or steel tendons.

In cases of unbonded tendons, on the other hand, beams with FRP and steel tendons behave very similarly [8-10]. The only difference is FRP tendons showed linear behaviour up to the ultimate load and have lower elastic modulus as compared to steel tendons. Pisani [10] numerically analysed simply supported beams prestressed with unbonded GFRP or steel tendons and stated that the beams with unbonded GFRP tendons showed non-linear load-deflection behaviour up to ultimate load, which was very similar to that of the unbonded steel tendons beams. The ductility of the GFRP beams was even better, although their ultimate strength was lower than beams reinforced with steel tendons. Similar observations were also reported by Lou et al. [8] for beams externally prestressed with FRP tendons. Tan and Tjandra [9] tested continuous beams and concluded that the use of external CFRP tendons did not lead to significant differences in the ultimate loads, tendon stresses, and deflections as compared to conventional steel tendons.

When FRP tendons are used for prestressing, stress concentration in the tendon due to harping effect is an important factor that needs due care. The localized curvature generated by the deviation will cause a high stress concentration in the tendons which adversely prevents the tendons to fully achieve its breaking capacity. The effects of the deviator curvature, harped angle, and tendon size are found to be the main factors impacting the stress increment in the CFRP tendons accounting for the harping effect [11-14]. Mutsuyoshi and Machida [11] found that CFRP tendons deviated at an angle of 11.3^{o} ruptured at approximately 80% of their breaking load when 400-mm diameter steel deviators were used. Grace and Abdel-Sayed [12] reported 19% and 34% reductions in breaking forces for carbon fiber composite cable (CFCC) tendons draped at 3° angle and 5° angles when using 50.8 mm diameter deviators. When 508 mm diameter deviators were used, those reductions were 12% and 26% at draping angles of 5° and 10°, respectively. Quayle [13] found reductions ranging between 13% and 50% in the tensile strength of the CFRP tendons when the tendons were draped at 2° to 15° with 50 mm to 1000 mm radii deviators, respectively. Based on finite element analysis on Basalt FRP tendons, Wang et al. [14] recommended a bending angle less than 3° to avoid the strength reduction percentage exceeding 10%.

Joints between segments are the most critical part of PSBs as they permit the shear transfer and integrity of the whole structure. The joints can be epoxied or dry, flat or keyed, and having single or multiple shear keys and are made of plain concrete or reinforced concrete. The behavior of joints under direct shear were extensively studied in the literature [15-17]. From experimental tests on panels, Turmo et al. [17] concluded that the use of steel fibre reinforced concrete (SFRC) did not increase the shear capacity of the panel joints. In addition, the formulation recommended by AASHTO [18] yielded the best prediction for the shear capacity of the joints as concluded by the authors.

This different feature between a segmental and a monolithic beam may cause further concern to the PSBs as the opening of joint and sliding of segments may cause stress concentration in the tendon and change the loading distributions in the beam. This, in turn, raises up a question, is FRP tendon a good solution for prestressing PSBs despite owning excellent mechanical properties? In other words, can the FRP tendon fully achieve its breaking capacity or will it suffer from premature failure due to stress concentration at joint locations? Since FRP tendon is made of an anisotropic material, it has very low transverse modulus and strength as compared to those in the longitudinal direction.

This study, therefore, focuses on investigating the behaviour of PSBs prestressed with unbonded CFRP tendons. As far as the authors are aware, this is the first time CFRP tendons are applied to post tensioning segmental concrete beams. The effect of tendon types and joint types on the structural behaviour of segmental concrete beams will be discussed.

2 Experimental program

To evaluate the use of CFRP tendons on PSBs, three large scale segmental concrete beams including two beams post-tensioned with CFRP tendons and one beam with unbonded steel tendons which served as a reference specimen were built and tested in the Civil Engineering Laboratory, Curtin University. Two types of dry or epoxied multiple shear-keyed joints were used in the beams. All the beams were then tested under four-point loading test up to failure. The details of specimen design and test set up are described in the subsequent sections.

2.1 Design of specimens

All the specimens were made of reinforced concrete and were designed according to the requirements of AASHTO [18] for segmental concrete beams and ACI 440.4R [4] for beams prestressed with FRP tendons. The total length of a beam is 3.9 m with T-shape cross-section of 400 mm height. Each beam consisted of four individual segments which were connected together by two steel or CFRP tendons using the posttensioning technique. For convenience, each specimen was labelled as given in Table 1, in which Beam BS1 was prestressed with two steel tendons and had dry joints while Beams BC1 and BC2 was prestressed with CFRP tendons with different joint types, i.e., dry or epoxied. Fig. 1 shows the design details and dimensions of the tested beams.

Previous studies showed that the shear stress distribution in the multiple shear-keyed joints, which are widely used in practice, is more uniform than in the single keyed joints [15, 16, 19]. As such, multiple shear-keyed joints were adopted in the present study. These shear keys had the same cross-section size but different lengths on the flange and on the web of the specimens as shown in Fig. 2.

Each segment of the beams was reinforced with the minimum amount of non-prestressed reinforcement at the top and bottom of the segment. This minimum amount reinforcement was in accordance with the requirements of ACI 318-14 [20] for beams with unbonded tendons. The minimum area of the longitudinal reinforcement was computed as: $A_{s,min} = 0.004A_{ct}$, where A_{ct} is the area of that part of the cross-section between the flexural tension face and the centroid of the gross section. Two 12 mm diameter deformed bars were used for the bottom longitudinal reinforcement and four 10 mm diameter deformed bars were used for the top layer. These steel bars were cut off leading to the discontinuity of the longitudinal steel reinforcement at each joint location. 10 mm diameter deformed bars were also used for transverse reinforcements which were placed at 100 mm spacing for the two middle segments and at 75 mm spacing for the two end segments to strengthen beams in shear (Fig. 1).

All the beams were under-reinforced according to strength design [18]. Beam BS1 has an unbonded prestressing reinforcement ratio of $0.112\rho_b$, while those of Beams BC1 and BC2 are $0.53\rho_b$ and $0.58\rho_b$, respectively. It is noted that ρ_b is the balanced prestressing reinforcement ratio for an counterpart beam with bonded tendons, which was given by ACI 440.4R [4] and presented in Eq. 1:

$$\rho_b = 0.85\beta_1 \frac{f_c^{'}}{f_{pu}} \frac{\varepsilon_{cu}}{\varepsilon_{cu} + \varepsilon_{pu} - \varepsilon_{pe}} \quad (1)$$

where f'_c is the compressive concrete strength, ε_{cu} is the ultimate compressive strain of concrete and taken as 0.003, f_{pu} and ε_{pu} are the design ultimate tensile strength and the corresponding strain of CFRP tendon, respectively, and ε_{pe} is the effective strain in the CFRP tendon caused by initial effective stress f_{pe}. It is noted that f_{pu} and ε_{pu} are replaced by the yield strength and the corresponding strain of steel tendons when calculating the balanced reinforcement ratio for

Beam BS1.

2.2 Materials

Pre-mixed concrete was used in this experiment and was supplied by a local supplier. Determination of concrete properties was conducted according to the Australian Standards AS 1012.8.1 [21] and AS 1012.9 [22] for concrete cylinders. The cylinders were of 100 mm diameter and 200 mm height. The average compressive strength of three concrete cylinders on the testing day was 44 MPa with a standard deviation of 1.47. Conventional steel bars of 12-mm and 10-mm diameters were used for longitudinal and transverse steel reinforcements, respectively. The ultimate tensile strength of 12-mm deformed bars N12 and 10-mm deformed bars N10 were 587 MPa and 538 MPa, respectively, as provided by the manufacturer. 7-wire 12.7-mm diameter steel tendons and single strand 12.9-mm diameter CFRP tendons were used in the specimens. The CFRP tendons were supplied by Dextra Building Products (GuangDong) CO., LTD [23]. The mechanical properties of the CFRP tendons were reported by the manufacturer after testing 16 CFRP coupons. Detailed properties of the materials used in the specimens were given in Table 2.

2.3 Casting of specimens

Steel cages of each segment of all beams were prepared and placed in a timber formwork. Corrugated metal duct of 40-mm diameter which was cut in designed length was also installed into the steel cages to create holes for placing tendons later. To separate each segment during pouring concrete, T-shape timber plates having the same dimension as beam’s cross-section were cut and placed in the formwork at intended locations as separation plates. Foam blocks were attached to the separation plates to form the shear keys as shown in Fig. 3.

All segments were cast using match-casting method, i.e. the first and third segments were cast in the first concrete batch, and then they were used as a formwork in the second batch to make the second and fourth segments. By this way, it ensured the male and female keys perfectly fit between two adjacent segments. Cylinders (100 mm diameter and 200 mm height) were also cast to determine the concrete properties.

After casting, all the segments were cured in a moist condition in which wet hessian rags were placed on top of the segments and were watered twice a day to keep them moist. The formwork was removed after 7 days of casting, then the segments were left for continuous curing at least 28 days before post-tensioning and testing. Fig. 3 shows a typical segment at completion.

2.4 Post-tensioning and epoxy

Fig. 4 shows a photo of typical set up of post-tensioning. One end of CFRP tendons was connected to a steel tendon via steel couplers as shown in Fig. 5. By this way, the prestressing procedure for the CFRP tendons was done similarly to the steel tendons. It is noted that this anchor design was made to ensure the tendon failure not to occur at the anchor region which was therefore not a concern of this study. The stressing force was generated by a monostrand hydraulic jack of 30 tons that seated onto a jacking chair. Two sets of wedges and barrel anchors were used in the stressing end, in which one was placed after the hydraulic jack called post-tensioning anchor #2 and another one was placed before the jack called working anchor #1. Hollow bolts and nuts (tightening system) were placed inside the jacking chair just before the working anchor for tightening and releasing the force later. 20-ton capacity load cells were used to measure the tensioning force generated by the hydraulic jack and the force in the tendon during the test.

For Beam BC2 with epoxied joints, the concrete surfaces of the shear keys were thoroughly cleaned using a steel brush and an air gun to make sure the surface in a good condition and free from dust. The concrete surfaces were then thoroughly watered and left to dry for at least 2 hours before applying the adhesive. A thin layer of Sikadur-30 [24] was applied to the joint surfaces of the segments using a trowel. After posttensioning, the epoxied beam was left for curing of the adhesive for 3 days.

The stressing procedure was done as follows. In the first step, the tendons were stressed an initial force of approximately 10% of the total stressing force, F_s, to close the gaps between segments and to remove the slack. F_s was computed from the control stress in the tendons, which were taken as 0.75 f_{pu} for steel tendons [18] and 0.4 f_{pu} for CFRP tendons [4]. Then each tendon was stressed in three load levels at 20%, 60% and 100% of the total stressing force until completion. Load cells and strain gauges attached to the tendons were used to monitor and measure the stresses in the tendons during the post-tensioning process. The effective tendon stresses and the corresponding force in the tendons immediately following transfer are listed in Table 1.

2.5 Measurements, test set up and loading

Measurements recorded during the tests include the applied load, vertical displacement, opening of joints, strain in prestressing tendons and non-prestressing rebars. The applied load was monitored by load cells attached to the hydraulic jacks. The load cells were calibrated to have less than 1% error at the maximum loading capacity of 40 tons, and the error was smaller at lower range, usually 0.5% to 1%. Linear variable differential transformers (LVDTs) of 100 mm measurement range were used for tracking the vertical displacement and opening of joints. The accuracy of the LVDTs was around 0.5% to 1% over 100 mm span. Strain in the rebars and prestressing tendons were measured by strain gauges and load cells attached at the end of the beams as shown in Fig. 6. FLA-2 series of strain gauges supplied by Bestech Company [25] were used in the tests.

The applied load was exerted by two vertical hydraulic jacks of 55 tons each placed equally at one-third span. Two horizontal I steel beams were used to uniformly transfer the vertical loads from the jacks to the beams. All the beams were tested under monotonic loads progressively up to failure and the progressive loading pattern is shown in Fig. 7. Two load cycles were performed at each loading level. The load increment in each loading level was 20 kN. In each cycle, the applied load was gradually increased to the designated value of that loading level and then was reduced to around 5 kN before starting the next cycles, except the first loading cycle when the applied load started from 0. All the tests were carried out under load control at a rate of 3 to 5 kN/min.

3 Experimental results

3.1 Failure modes

The tested results of all the specimens are shown in Table 3 in which P_y, P_u, $\delta_{mid,y}$, $\delta_{mid,u}$, $\Delta_{J,y}$, $\Delta_{J,u}$ are the applied loads, midspan deflections, and openings of the middle joint of the specimens at yielding and at ultimate condition, respectively. The definition of yielding point is given in Section 3.3.

The failure of all the tested beams is shown in Fig. 8. The failure started by concrete crushing on the top fibre followed by yielding of the steel tendons for Beam BS1 or rupturing of CFRP tendons for beams prestressed with CFRP tendons. The crushing of concrete and rupture of tendons occurred at the middle joint located at the midspan for all the beams. All the beams in this study were under-reinforced in regards to a counterpart beam with bonded tendons, therefore the failure mode would theoretically be tension controlled since $c/d < 0.42$ by AASHTO LRFD [26] or $c/d < 0.375$ by ACI 318-14 [20], where c is the depth of the neutral axis, d is the distance from the extreme top fibre to the centroid of tension force. However, the test results show concrete crushing failure. In fact, unbonded tendons shifted the failure mode of the under-reinforced counterparts from tension controlled to compression controlled. This phenomenon may be attributed to the fact that the strain in the unbonded tendons does not depend on the section analysis but the whole beam behaviour [27], which allows the beam to achieve larger deflection leading to the higher compression strain in the concrete on the top fibre. As a result, the calculation of the balanced reinforcement ratio for beams with unbonded tendons requires further consideration. Lee et al. [28] found that the balanced reinforcement ratio of a beam with unbonded tendons (ρ_b^U) was always smaller than that of a beam with bonded tendons (ρ_b^B) and the ratio of ρ_b^U / ρ_b^B varied in a range between 0.43 and 0.83 for specimens considered in their study.

3.2 Load-deflection curves

The load-deflection curves for all the specimens under four-point loading at different loading levels are shown in Fig. 9. The envelop curves of these relations are plotted in Fig. 10. As shown, Beam BC1 with unbonded CFRP tendons behaved very similar to Beam BS1 with steel tendons. In both cases, the load-deflection curves were divided into two stages by a transition zone. In the first stage, both beams had high stiffness and showed a linear relationship between the applied load and deflection. In the second stage, the beams' stiffness sharply reduced and the beams deformed in a non-linear manner up to failure. The transition from the first stage to the second stage is related to the opening of the middle joint J2 under the applied loads. As observed in Fig. 13, the middle joint J2 in Beams BS1 and BC1 started to open at the applied loads of approximately 43.3 kN and 40.1 kN, respectively. At the same time, the stiffness of the beams started to reduce dramatically. The only difference between the two beams was that Beam BS1 had a higher initial stiffness than Beam BC1. However, after cracking Beam BS1 showed a lower tangent stiffness because of its lower reinforcement index, $\omega_{ps} = \frac{f_c^{'}}{f_{pu}} \rho_{ps}$ where ρ_{ps} is the reinforcement ratio. This behaviour is similar to segmental beams prestressed with external steel tendons reported in previous studies [16, 29].

Similarly, the load-deflection curve of Beam BC2 with epoxied joints also exhibited two stages. However, in the second stage, the beam still deformed almost linearly with the applied load up to failure by rupture of the tendons. It is worth noting that the transition zone in the curve is the result of concrete cracking in tension at bottom fibre at a load of approximately 44.7 kN. The tensile crack was formed by one vertical crack cutting off all the shear-key bases of joint J2 located at midspan of the beam when the tensile stress generated by the applied load exceeded the tensile strength of the concrete (Fig. 8c). Further details on this type of cracking are discussed in the next section.

Type of joints also affected on the initial stiffness of the beams. As shown in Fig. 10, Beam BC1 with dry joints had a lower initial stiffness as compared to Beam BC2 with epoxied joints. This difference was resulted from the distinguished moment of inertia of the two beams in which Beam BC1 with dry joint had the moment of inertia much smaller than that of Beam BC2 associated with epoxied joints.

Previous studies [30, 31] showed that the response of monolithic beams with completely unbonded tendons (without any ordinary tension reinforcement) is quite different from that of beams with additional ordinary tension reinforcement as it behaves as a shallow tied arch after cracking rather than a flexural member. Beam BS1 in this study may be considered as a beam without any tension reinforcement as all the tension reinforcements were discontinued at joint locations, however, the load-deflection curve had a good performance as it showed an ascending branch after cracking. This is an additional benefit of segmental beams as compared to monolithic ones associated with internal unbonded tendons.

3.3 Ductility

It is seen in Fig. 9 and Fig. 10 that all the specimens achieved large deflection before complete failure. The maximum midspan displacement of Beam BS1 reached 89.4 mm which was equal to 1/40 of the span length, L_b. The maximum midspan displacements of Beams BC1 and BC2 were 94.7 and 101.1 mm, corresponding to 1/38 and 1/35 L_b, respectively. It is noted that the maximum allowable midspan displacement of these beams is L_b/800 according to AASHTO LRFD [26]. These deflection capacities ensure to give engineers warnings before failure or total collapse of the structures.

To reflect the physical behaviour of the tested beams in terms of ductility indices, two calculation methods for the ductility of the beams, namely displacement ductility and energy ductility were adopted in this study: Method 1, $\mu = \frac{\Delta_u}{\Delta_y}$ and Method 2, $\mu = \frac{A_u}{A_y}$, where Δ_u is the ultimate midspan deflection; Δ_y is the midspan deflection of the beam at yielding of tension steel; A_u is the area under the load-deflection curve at ultimate deflection, and A_y is the area under the load-deflection curve at yielding of steel. The definition of yield point proposed by Park [32] was adopted in this study and was illustrated in Fig. 11. The yielding of the structure was due to the joint opening in cases of beams BS1 and BC1 and the concrete cracking in the tension zone at beam's soffit in the case of Beam BC2. The ductility of the beams is presented in Table 4.

It is seen from Table 4 that both the displacement ductility and energy ductility of Beam BS1 are higher than those of Beam BC1 although Beam BC1 achieved the maximum displacement at 94.7 mm which was even larger than that of Beam BS1. The ductility of Beam BC2 is approximately 3 times higher than that of Beam BS1. It can be noted that both the beams with CFRP tendons have higher displacement capacity, and the ductility is governed by the yielding displacement. This observation has proven that CFRP tendons can be used to replace steel tendons to achieve the required strength and possibly even better ductility for segmental beams.

Interestingly, Beam BC2 had a ductility approximately 4 times higher than that of Beam BC1 as given in Table 4. However, it can be observed from Fig. 10, Beam BC1 showed similar strength and deflection capacities as beam BC2. The reason for this big difference is due to the variation in the value of the equivalent displacement at the yielding point. As shown, Beams BC1 and BC2 had relatively similar maximum displacements and strengths but their yielding points were different leading to the 4 times difference in ductility. It means that the ductility of these beams is significantly governed by the displacement at the yielding point which can only be approximately obtained from the testing data. The definition and calculation of ductility of PSB beams prestressed with CFRP tendons with dry or epoxied joints need further verification.

4 Discussions

4.1 Joint openings

Fig. 12 shows the opening of all joints along beam's axis at the ultimate state. It can be seen from the curves that in all the beams only the middle joints (J2) opened while the other joints (J1 and J3) almost remained closed under the ultimate loads and the magnitude of the opening at the ultimate load was nearly equal regardless of the types of joint used. This observation confirms the assumption that the beam develops one major crack at the midspan at the ultimate stage, which can be used to calculate the plastic hinge length and the stress in the unbonded tendons in several models [33-35]. These models assumed that the tendon elongation occurred only at the opening hinge at the midspan of the beam. The opening of the middle joint at the ultimate state for Beams BS1, BC1 and BC2 was 30.44 mm, 27.70 mm and 30.02 mm, respectively.

The opening of the middle joint J2 with respects to the applied loads for all the beams was plotted in Fig. 13. It can be seen from the figure that the shapes of the applied load-joint opening curves are very similar to the curves of the applied load and deflection for all the beams as shown in Fig. 10. At the beginning, the joint still remained closed by the time it reached the opening load or cracking load as discussed previously. After that, the joint started to open at a much larger rate leading to the sudden reduction in the stiffness of the beams.

It is worth mentioning that the opening of joint J2 in Beam BC2, in fact, was the development of a flexural vertical crack cutting off all shear-keyed bases as shown in Fig. 8c. The flexural crack started from the bottom and quickly propagated to a certain height of the joint. This phenomenon is because the tensile strength of the adhesive was much higher than the tensile strength of concrete (20 MPa vs ~4 MPa) and there was no ordinary steel rebars through the joint. After cracking, the middle joint in the epoxied beam behaved similarly to those in dry joint specimens as seen in Fig. 12. It is noted that all joints completely closed when the load was released at the end of each load level as the effect of prestressing.

The relationships between the joint opening and midspan deflection for specimens are plotted in Fig. 14. It can be clearly seen from the figure that for all the specimens the joint showed an almost linear relationship with the midspan deflection. Therefore, it can be stated that the width of the vertical crack in case of the epoxied beam developed linearly with the midspan deflection under the applied load. The joint opening was also plotted against the tendon stress in Fig. 15. It is seen from the figures that in Beams BC1 and BC2, the stress in the CFRP tendons increased approximately linearly with the joint opening up to ultimate stage. Meanwhile, Beam BS1 showed a non-linear relationship between the tendon stress and the joint opening. This observation suggests the calculation of stress in the unbonded tendons of a segmental beam based on the deflection of the beam by assuming the elongation of the tendon is equal to the opening of the joint.

4.2 Stress development in the tendon under applied load

Fig. 16 shows the evolution of the prestressing tendon stress under four-point loading. The corresponding envelop curves are plotted in Fig. 17. The effective stresses in the tendon at the beginning of the loading process for beams BS1, BC1, and BC2 were 1280 MPa, 818 MPa and 661 MPa, respectively. It is seen from the figure that the tendon stress in all the beams started to increase from the beginning of the test. The increase in the tendon stress was due to the deflection of the beam under applied loads as such the applied load and tendon stress curves are very similar to the curves of the applied load and deflection. From the figure, it can be seen that the applied load vs tendon stress of the beams with CFRP tendons showed a bilinear relationship but not for the beam with steel tendons. The one with steel tendon showed a highly non-linear behaviour. It means the stress in the CFRP tendons increased nearly linearly to the applied load, but with different increase rate before and after joint opening.

The tendon stress at the ultimate load in Beam BS1 was 1748 MPa, which was equal to 94% of the nominal tensile strength of the prestressing steel tendons (1860 MPa). It is worth mentioning that the test for Beam BS1 was stopped for the safety reason when large physical damage was observed in the concrete on the top fibre (Fig. 8a). At that time, the prestressing steel tendons already yielded but had not ruptured yet. After releasing the applied load, the beam still recovered a certain deformation due to the retraction of steel tendons. In both Beams BC1 and BC2, the CFRP tendons ruptured at the ultimate load. The tendon stresses at rupture were 1774 MPa and 1687 MPa for Beams BC1 and BC2, respectively. It is worth noting that these stress values were far below the nominal breaking strength of the CFRP tendon as they were only equal to 72% and 69% of the breaking strength which was 2450 MPa as reported by the manufacturer after carrying out 16 coupon tensile tests. This reduction in the tensile strength of the CFRP tendons was affected by the loading type (bending loading), harping effect, and the joint opening. Harped angle greatly prevents the increase in the tendon stress as shown in previous studies [11-14]. In this study, a harping angle of 3° was used to avoid the strength reduction exceeding 10% as recommended by Wang et al. [14]. Therefore, the joint opening was responsible for low stress increment in CFRP tendons which requires further investigation.

After joint opening, the beams deformed at a much faster rate under the applied load so that the increase in the tendon stress was much larger than that in the first stage when the beams were still in the elastic region (Fig. 18). The total tendon stress increment in Beam BS1 was 468 MPa, which equals $0.25f_{pu}$ and those in Beams BC1 and BC2 were 956 MPa and 1026 MPa, which equal $0.33f_{pu}$ and $0.27f_{pu}$, respectively (Table 5).

4.3 Tendon stress increment versus midspan deflection

Fig. 19 shows the relationship between the tendon stress and vertical displacement of the beams. It is seen from the curves that in all the beams, the tendon stress increment exhibited an approximately linear relation to the midspan deflection up to the ultimate load regardless of the type of tendons used. Even though, there was a slight variation in the curves of beams BS1 and BC1 after joint opening. This observation is similar to previous studies conducted on monolithic beams prestressed with unbonded tendons. Experimental tests by Tao and Du [30] showed that there exists such linear relationship for moderately reinforced partially prestressed concrete beams with unbonded steel tendons. Lou and Xiang [31] confirmed this observation based on their numerical analysis. Wang et al. [14] also found this linear relationship between tendon stress increment and midspan deflection when conducting tests on beams externally prestressed with BFRP tendons. As such, this observation confirms the calculation procedure for stress increment in the PSB prestressed with unbonded CFRP tendons based on midspan deflection which have been used for monolithic beams [36, 37].

4.4 Strain in rebars

Since all the beams showed similar behaviour regarding the strain evolution in the ordinary steel rebars under the applied loads, only the experimental results of Beam BS1 was given in Fig. 20 for brevity, where R1 and R2 are the strains in the bottom and top longitudinal rebars; R3, R4 and R5 and R6 are the strains in the stirrups of segment No.2 near middle joint J2, and joint J3 as shown in Fig. 6, respectively. At the beginning, the strain in the top bars (R2) was almost zero, while the bottom longitudinal bars were in compression with a strain of around -300 μm/m resulted from prestressing. When loads were applied, the top bars started to be compressed, however, the strain developed in the bars at the ultimate stage was very small since the strain gauge was attached in the middle of the segment which was far from the failure position. Meanwhile, the stress in the bottom bars gradually changed from compression to tension at cracking. The strain in the bottom bars was also very small at the ultimate load at around 100 μm/m, which is far below the yielding point. This indicates that there is very small contribution of longitudinal reinforcement bars to the loading capacity of segmental beams. Yuan et al. [38] and Jiang et al. [39] reached the same conclusion in their studies on segmental beams prestressed with steel tendons.

Steel stirrups near joint J2 developed a very small strain since J2 was in the pure bending region under loading. The strain in the stirrups near J1 was also very small, even though J1 was in the region with combined shear and bending. This indicates that the stirrups contributed little to resisting the shear force at the joint locations as was also reported in the previous study [16].

4.5 Residual displacement

Fig. 21 shows the residual displacement at the end of each loading level of the specimens. It can be seen from the figure that at the end of the load level just onset of the failure, the beams prestressed with CFRP tendons underwent lesser residual displacement than the beam with steel tendons. Beam BS1 underwent 8.06 mm residual displacement (0.22% L_b), while those for Beams BC1 and BC2 were 5.47 mm (0.15% L_b) and 1.61 mm (0.04% L_b), respectively. However, before opening of the joints, Beam BS1 had better performance than Beam BC1 as it showed a smaller residual displacement after each load level. After joint opening, the residual displacement sharply increased at the end of each load level in Beam BS1. Meanwhile, the residual displacement in beam BC1 approximately increased linearly from the first to the last loading level. As can be seen that replacing steel tendons by CFRP tendons resulted in a better self-centring capacity of a PSB in which the beam could recover close to its original position after excessive loading, for example from overloaded trucks.

Moreover, the epoxied joints greatly affect the behaviour of the beams with regards to the residual deflection. It can be seen from the figure that beam BC2 underwent much lesser residual deflection than Beam BC1. The experimental results have shown that the epoxied joints can be used to achieve better self-centring capacity.

5 Analytical calculations

In this section, the accuracy of the current design procedures and equations recommended for the calculation of the unbonded tendon stress at the ultimate load is evaluated. The examined codes include AASHTO [18] , ACI 440.4R [4], ACI 318-14 [20] and BS 8110 [40]. However, it is noted that except AASHTO [18], the equations for calculating tendon stress, f_{ps}, recommended by these codes are developed for the analysis of monolithic concrete beams, no equation is provided in these codes to address segmental beams prestressed with unbonded CFRP tendons. The design procedure presented in AASHTO [18] is used for segmental beams prestressed with steel tendons. ACI 440.4R [4]'s equations are developed for monolithic beams with CFRP tendons. ACI 318-14 [20] and BS 8110 [41] are for monolicthic beams with steel tendons. In brief, there is no specific design guide yet for segmental beams prestressed with CFRP tendons.

For convenience, symbolic for the same parameter in different codes is modified to be identical.

AASHTO [18] adopted the following equation to predict the average stress in the unbonded tendons in precast segmental concrete beams:

$$f_{ps} = f_{pe} + 6200\left(\frac{d_{ps} - c}{l_e}\right), MPa \quad (2)$$

where f_{ps} is the effective tendon stress, d_{ps} is the distance from extreme top fibre to centroid of prestressing tendons, $l_e = L/(1+[N/2])$, in which L is the length of the tendon between anchorages, and N is the number of support hinges required to form a mechanism crossed by the tendon. The formula is based on the work of McGregor's research [35]. Up to date, there has been no recommendation by AASHTO [18] for FRP tendons in PSBs.

ACI 440.4R [4] recommended the following equation to predict the stress in CFRP tendons based on the work of Naaman et al. [41]:

$$f_{ps} = f_{pe} + \Omega_u E_{ps} \varepsilon_{cu}\left(\frac{d_{ps}}{c_u} - 1\right) \quad (3)$$

where E_{ps} is the tendon modulus of elasticity; ε_{cu} is the ultimate concrete compression strain which was taken as 0.003; c_u is the neutral axis depth at ultimate loading; and Ω_u is a strain reduction coefficient defined as $\Omega_u = 1.5/(L_b/d_{ps})$ for one-point midspan loading and $\Omega_u = 3/(L_b/d_{ps})$ for uniform or third-point loading, in which L_b is the span length. It is noted that Eq. 3 was also used to calculate the stress in the unbonded steel tendons as it was originally developed for beams with steel tendons [4]. A limitation of 0.94 f_{py} was recommended in Eq. 3 by Naaman and Alkhairi [27] based on the observation of experimental results, where f_{py} is the yield strength of steel tendons.

ACI 318-14 [20] suggested the following equation which is based on the research performed by Mattock et al. [42]:

$$f_{ps} = f_{pe} + 69 + \frac{f_c^{'}}{100\rho_{ps}}, MPa \quad (4)$$

where ρ_{ps} is the prestressing reinforcement ratio. This equation is applicable to beams with

$L/d_{ps} \leq 35$.

BS 8110 [41] recommended the following equation:

$$f_{ps} = f_{pe} + \frac{7000}{\frac{L}{d_{ps}}}\left(1 - 1.7\frac{f_{pu}A_{ps}}{f_{cu}bd_{ps}}\right), MPa \quad (5)$$

where A_{ps} is the area of prestressing tendons and f_{pu} is the nominal tensile stress at ultimate loading of the tendon, b is the width of the cross-section, and f_{cu} is the cube strength of concrete taken as $f'_c/0.8$.

The analytical and experimental results of the tendon stress and load capacity at ultimate condition for all the specimens are listed in Table 5. The accuracy comparison of analytical prediction of all code equations is shown in Fig. 22 and Fig. 23. As can be seen from Fig. 22, all the code equations predicted well the ultimate stress for Beam BS1 with unbonded steel tendons. It is worth mentioning that the result from Eq. 3 was taken as 0.94 f_{py} as recommend by Naaman and Alkhairi [27] because the stress value from Eq. 3 was higher than 0.94 f_{py}. This value from Eq. 3 was, however, too conservative since in the test the steel tendons in Beam BS1 already yielded. Results from AASHTO [18], ACI 318-14[20], and BS 8110 [41] equations are a bit larger than the experimental result for Beam BS1 since the test was stopped for safety reason as mentioned previously.

The accuracy of the design equations in these codes considerably reduced in cases of the beams with CFRP tendons as these codes are not specified for segmental beams with CFRP tendons. AASHTO [18] and BS 8110 [41] equations underestimated f_{ps} by about 22% for Beam BC1 with dry joints and 28% for Beam BC2 with epoxied joint as compared with the experimental results. ACI 318-14 [20] yielded the most conservative predictions at 31% and 36% lower than the experimental results for Beams BC1 and BC2, respectively. Again, ACI 440.4R [4]'s equation overestimated f_{ps} for both Beams BC1 and BC2 (Fig. 22). This is not common for a code equation since a code normally yields conservative results. The reason for this substantial difference may lie on the ratio L/d_{ps}. ACI 440.4R [4] limits the application of Eq. 3 for beams with CFRP tendons having an unbonded length greater than 15 times the depth of the beam. In this study, the ratio of unbonded tendon length to beam depth was equal to 9.

Similarly, except ACI 440.4R [4], all code equations predicted well P_u for beams with steel tendons but less accurate when CFRP tendons were used. P_u predicted by AASHTO [18] and BS 8110 [41] equations were respectively 18% and 16% lower than the experimental results for the beams with dry joints, while those for the beams with epoxied joints were worse at 33% and 31%, respectively. ACI 318-14 [20] underestimated P_u by 26% in the case of dry joint and 40% in the case of epoxied joints, respectively. ACI 440.4R [4] highly overestimated P_u due to the fact that the L/d_{ps} used in this study was lower than the code's recommendation.

In order to verify the sensitivity of L/d_{ps} to the increase in the tendon stress of the tested beams against the code equations, an analysis was made by plotting the tendon stresses computed by the code equations against L/d_{ps} for all specimens. Only L/d_{ps} ratio was assumed to vary between 7 and 45 while the other characteristics of the tested beams were kept constant. The curves are shown in Fig. 24 for the case of beams with steel tendons and in Fig. 25 for beams with CFRP tendons.

It can be seen from Fig. 24 that the change in the tendon stress is considerly influenced by the ratio of L/d_{ps} in all codes, except ACI 318-14 [20] where the tendon stress at ultimate loading only depends on f_{pe}, f'_c and ρ_{ps} as seen in Eq. 4. The increase in L/d_{ps} leads to the decrease in the f_{ps}. As discussed previously, all codes predicted closely to the experimental results of Beam BS1, except the prediction by Eq. 3. As such, the limitation of 0.94 f_{py} was used in the calculation.

From Fig. 25, similar trend is observed between f_{ps} and L/d_{ps} for beams with CFRP tendons by all codes. AASHTO [18], BS 8110 [41], and ACI 318-14 [20] underestimated the stress in the tendon at ultimate condition. In which AASHTO [18] and BS 8110 [41] yielded similar predictions, while ACI 318-14 [20] returned the least conservative result. ACI 440.4R [4] overestimated f_{ps} at ultimate loading, however, both code prediction and experimental results were far below the nominal breaking strength of the tendons. Therefore, the strain reduction coefficient used by ACI 440.4R [4] in Eq. 3 is modified to $\Omega_u = 2.1 / (L/d_{ps})$ based on the experimental results conducted in this study for segmental beams prestressed with CFRP tendons. The curve of the modified Eq. 3 is also shown in Fig. 25.

6 Conclusion

An experimental study was conducted to evaluate the application of CFRP tendons on precast segmental concrete beams. Three T-section segmental beams with either unbonded CFRP tendons or steel tendons were built and tested under cyclic loads. Assessment of the four code equations to predict the stress increment in the unbonded tendons was also presented. The main findings are summarized as follows:

1. CFRP tendons can be well in replacement of steel tendons for segmental concrete beams. They can assure the beams to achieve both good strength and ductility capacity.

2. The CFRP prestressed beam with dry joints performed similarly as the beam with unbonded steel tendons in terms of overall load and deflection curve. They both showed non-linear load and displacement relations after cracking. However, CFRP prestressed beams with epoxied joints showed a linear load and displacement relation up to failure.

3. Unbonded CFRP tendons shifted the failure mode of under-reinforced beams from tension controlled to compression controlled. This transition in the failure modes may prevent the beams from a brittle failure manner when sudden rupture of the CFRP tendons in tension

occurs.

4. Epoxied or dry joints greatly affected the initial stiffness of the beams but had no effect on the joint opening under the applied loads after cracking.

5. The average stress in the unbonded CFRP tendons for the beams with dry joints and epoxied joints was only 72 % and 69% of the nominal tensile strength, respectively. The reduction in the tendon stress at ultimate loading might be governed by the loading type, harping effect and the joint opening which requires further investigation.

6. All the examined codes in this paper predicted well the unbonded steel tendon stress at ultimate condition, however, the accuracy significantly reduced when CFRP tendons were used. AASHTO [18] and BS 8110 [41] equations yielded better prediction among others, but underestimated f_{ps} by approximately 22% for Beam BC1 with dry joints and 28% for Beam BC2 with epoxied joint compared to the experimental results. A modification of ACI 440.4R [4] code equation was suggested for segmental beams prestressed with unbonded CFRP tendons to predict the stress in the tendon at ultimate loading.

7. Even though all the beams achieved similar deflection at the ultimate loading, the ductility calculation showed large difference among these specimens. The reason might be due to the sensitivity in determining the equivalent yielding point.

7 Acknowledgements

The authors would like to thank staff at the Civil Engineering laboratory, Curtin University, especially Mr. Mick Elliss for their technical help during the experimental program. Thanks are also expressed to Jaxier Koa and Xyrus Dangazo, final-year students for their great help in the experimental works. Finally, the first author would like to acknowledge the Curtin Strategic International Research Scholarship (CSIRS) and Centre for Infrastructural Monitoring and

Protection, School of Civil and Mechanical Engineering, Curtin University for the support of his full PhD scholarship. The first author would also like to thank Hong Duc University, Thanh Hoa, Vietnam for the support during his study course.

Notation

A_{ct}	area of the cross-section part between the flexural tension face and the centroid of the gross section
A_{ps}	area of prestressing tendons
A_u	area under the load-deflection curve at ultimate deflection
A_y	area under the load-deflection curve at yielding of tension steel
b	width of the cross-section
c	neutral axis depth of the section
c_u	neutral axis depth of the section at the ultimate condition
d	distance from the extreme top fibre to the centroid of tension force
d_{ps}	distance from extreme top fibre to centroid of prestressing tendons
f'_c	compressive concrete strength
f_{cu}	cube strength of concrete
f_{pe}	effective stress in the prestressing tendons after transfer
f_{pu}	ultimate tensile strength of prestressing tendons
f_{py}	yield strength of steel tendons
L	length of the tendon between anchorages
L_b	effective span length of the beam
N	number of support hinges
P_u	applied load at the ultimate loading condition
P_y	applied load at yielding
$\Delta_{J,u}$	opening of the middle joint at the ultimate loading condition
$\Delta_{J,y}$	opening of the middle joint at yielding
$\delta_{mid,u}$	midspan deflection at the ultimate loading condition
$\delta_{mid,y}$	midspan deflection at yielding
Δ_u	midspan deflection of the beam at the ultimate condition
Δ_y	midspan deflection of the beam at yielding of tension steel
ε_{cu}	ultimate compression strain of concrete
ε_{pe}	effective strain in the prestressing tendons
ε_{pu}	ultimate tensile strain of prestressing tendons
ρ_b, ρ_b^B	balanced reinforcement ratio of a beam with bonded tendons
ρ_b^U	balanced reinforcement ratio of a beam with unbonded tendons
ρ_{ps}	prestressing reinforcement ratio
ω_{ps}	reinforcement index
Ω_u	strain reduction coefficient

8 References

[1] Woodward R, Williams F. Collapse of YNS-Y-GWAS Bridge, Glamorgan. Proc Inst Civ Eng 1988;84(4):635-69.

[2] Wouters J, Kesner K, Poston R. Tendon corrosion in precast segmental bridges. Transp Res Rec J Transp Res Board 1999(1654):128-32.

[3] Concrete Society Technical Report. Durable post-tensioned concrete structures. TR 72, 2002.

[4] ACI 440.4R. Prestressing concrete structures with FRP tendons. Farmington Hills, USA: American Concrete Institute; 2004.

[5] Dolan CW, Swanson D. Development of flexural capacity of a FRP prestressed beam with vertically distributed tendons. Compos B Eng 2002;33(1):1-6.

[6] Maissen A, de Smet CA. Prestressed concrete using carbon fibre reinforced plastic (CFRP) strands. Mater Struct 1998;31(3):175-7.

[7] Zou PXW. Flexural Behavior and Deformability of Fiber Reinforced Polymer Prestressed Concrete Beams. J Compos Constr 2003;7(4):275-84.

[8] Lou T, Lopes SMR, Lopes AV. Numerical analysis of behaviour of concrete beams with external FRP tendons. Constr Build Mater 2012;35:970-8.

[9] Tan KH, Tjandra RA. Strengthening of RC continuous beams by external prestressing. J Struct Eng 2007;133(2):195-204.

[10] Pisani MA. A numerical survey on the behaviour of beams pre-stressed with FRP cables. Constr Build Mater 1998;12(4):221-32.

[11] Mutsuyoshi H, Machida A. Behavior of Prestressed Concrete Beams Using FRP as External Cable. Spec Publ 1993;138:401-18.

[12] Grace NF, Abdel-Sayed G. Behavior of externally draped CFRP tendons in prestressed concrete bridges. PCI J 1998;43(5):88-101.

[13] Quayle TG. Tensile-flexural Behaviour of Carbon-fibre Reinforced Polymer (CFRP) Prestressing Tendons Subjected to Harped Profiles: MS thesis. Univ. Waterloo; 2005.

[14] Wang X, Shi J, Wu G, Yang L, Wu Z. Effectiveness of basalt FRP tendons for strengthening of RC beams through the external prestressing technique. Eng Struct 2015;101:34-44.

[15] Jiang H, Chen L, Ma ZJ, Feng W. Shear Behavior of Dry Joints with Castellated Keys in Precast Concrete Segmental Bridges. J Bridge Eng 2015;20(2):04014062.

[16] Li G, Yang D, Lei Y. Combined shear and bending behavior of joints in precast concrete segmental beams with external tendons. J Bridge Eng 2013;18(10):1042-52.

[17] Turmo J, Ramos G, Aparicio AC. Shear strength of dry joints of concrete panels with and without steel fibres. Application to precast segmental bridges. Eng Struct 2006;28(1):23-33.

[18] AASHTO. Guide Specifications for Design and Construction of Segmental Concrete Bridges, 2nd Ed with 2003 Interim Revis. Washington, DC: American Association of State Highway and Transportation Officials; 1999.

[19] Zhou X, Mickleborough N, Li Z. Shear strength of joints in precast concrete segmental bridges. ACI Struct J 2005;102(1):3.

[20] ACI 318-14. Building code requirements for structural concrete and commentary: American Concrete Institute. International Organization for Standardization; 2015.

[21] AS 1012.8.1. Methods of testing concrete - Method 8.1: Method for making and curing concrete—Compression and indirect tensile test specimens. Standards Australia International

Ltd, NSW 2014.

[22] AS 1012.9. Methods of testing concrete - Method 9: Compressive strength tests—Concrete, mortar and grout specimens. Standards Australia International Ltd, NSW 2014.

[23] Dextra Group. CFRP tendons. https://wwwdextragroupcom/offices/dextra-building-products-limited.

[24] Sika Australia. Sikadur-30. https://aussikacom/.

[25] Bestech Company. https://www.bestech.com.au/.

[26] AASHTO LRFD. Bridge Construction Specifications, 6th Edition, U.S. Units. Washington, DC: American Association of State Highway and Transportation Officials; 2012.

[27] Naaman AE, Alkhairi F. Stress at ultimate in unbonded prestressing tendons: Part 2—Proposed Methodology. ACI Struct J 1991;88(6):683-92.

[28] Lee C, Shin S, Lee H. Balanced Ratio of Concrete Beams Internally Prestressed with Unbonded CFRP Tendons. Int J Concr Struct Mater 2017;11(1):1-16.

[29] Saibabu S, Srinivas V, Sasmal S, Lakshmanan N, Iyer NR. Performance evaluation of dry and epoxy jointed segmental prestressed box girders under monotonic and cyclic loading. Constr Build Mater 2013;38:931-40.

[30] Tao X, Du G. Ultimate stress of unbonded tendons in partially prestressed concrete beams. PCI J 1985;30(6):72-91.

[31] Lou T, Xiang Y. Effects of ordinary tension reinforcement on the response of beams with unbonded tendons. Adv Struct Eng 2007;10(1):95-109.

[32] Park R. Evaluation of ductility of structures and structural assemblages from laboratory testing. Bull N Z Natl Soc Earthq Eng 1989;22(3):155-66.

[33] Harajli MH. On the stress in unbonded tendons at ultimate: Critical assessment and proposed changes. ACI Struct J 2006;103(6):803.

[34] Lee L-H, Moon J-H, Lim J-H. Proposed methodology for computing of unbonded tendon stress at flexural failure. Struct J 1999;96(6):1040-8.

[35] Roberts-Wollmann CL, Kreger ME, Rogowsky DM, Breen JE. Stresses in external tendons at ultimate. ACI Struct J 2005;102(2):206.

[36] He Z, Liu Z. Stresses in External and Internal Unbonded Tendons: Unified Methodology and Design Equations. J Struct Eng 2010;136(9):1055-65.

[37] Harajili M, Kanj M. Ultimate flexural strength of concrete members prestressed with unbonded tendons. Struct J 1992;88(6):663-74.

[38] Yuan A, Dai H, Sun D, Cai J. Behaviors of segmental concrete box beams with internal tendons and external tendons under bending. Eng Struct 2013;48:623-34.

[39] Jiang H, Cao Q, Liu A, Wang T, Qiu Y. Flexural behavior of precast concrete segmental beams with hybrid tendons and dry joints. Constr Build Mater 2016;110:1-7.

[40] BS 8110. Structural use of concrete. London: British Standards Institution; 1997.

[41] Naaman AE, Burns N, French C, Gamble WL, Mattock AH. Stresses in unbonded prestressing tendons at ultimate: Recommendation. Struct J 2002;99(4):518-29.

[42] Mattock AH, Yamazaki J, Kattula BT. Comparative study of prestressed concrete beams, with and without bond. J Proc 1971;68(2):116-25.

9 List of Figures

Fig. 20: Strain in rebars in Beam BS1

Fig. 21: Residual displacement of specimens

Fig. 22: Comparison of calculation of f_{ps}

Fig. 23: Comparison of calculation of Pu

Fig. 24: Relationship between f_{ps} and L/d_{ps} ratio for beams with steel tendons

Fig. 25: Relationship between f_{ps} and L/d_{ps} ratio for beams with CFRP tendons

10 List of Tables

List of Figures

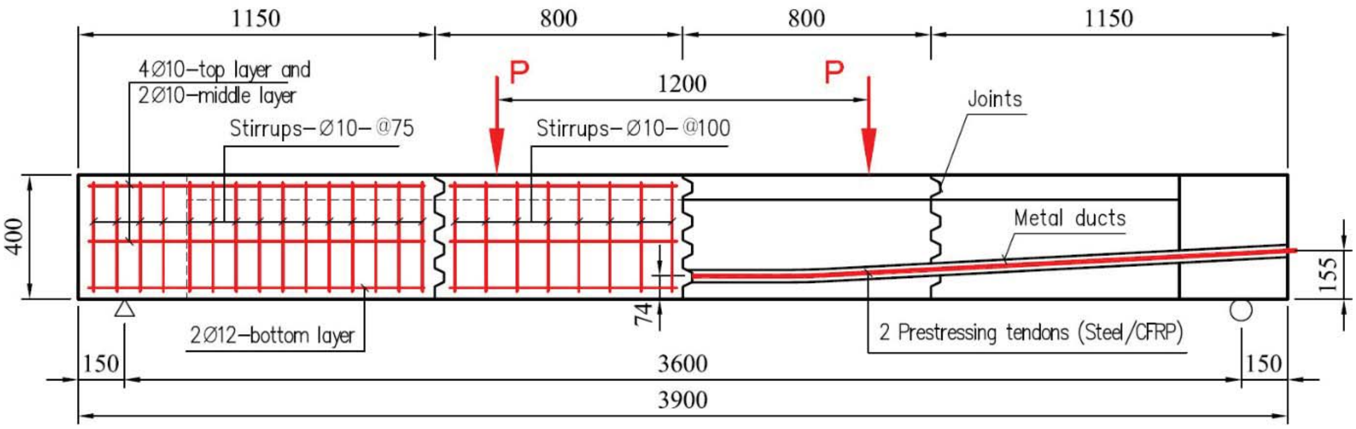

Fig. 1. Detailed dimensions of tested beams

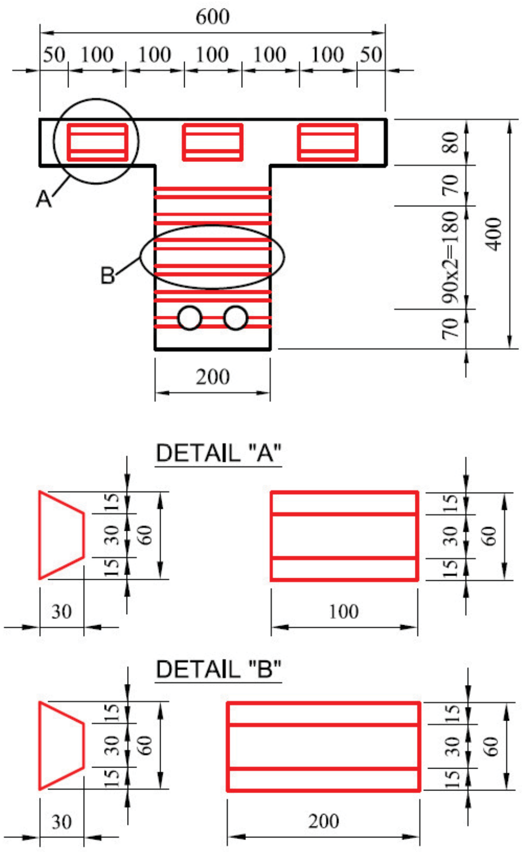

Fig. 2. Multiple shear-keyed joints

Fig. 3: Casting of specimens

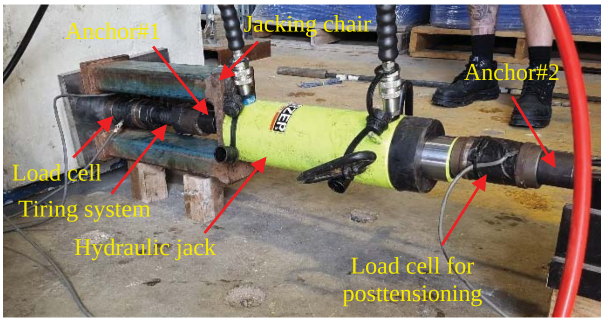

Fig. 4: Typical set up for post-tensioning

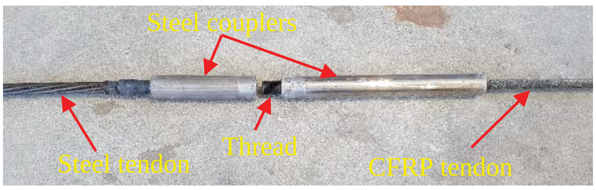

Fig. 5: CFRP tendon with steel couplers

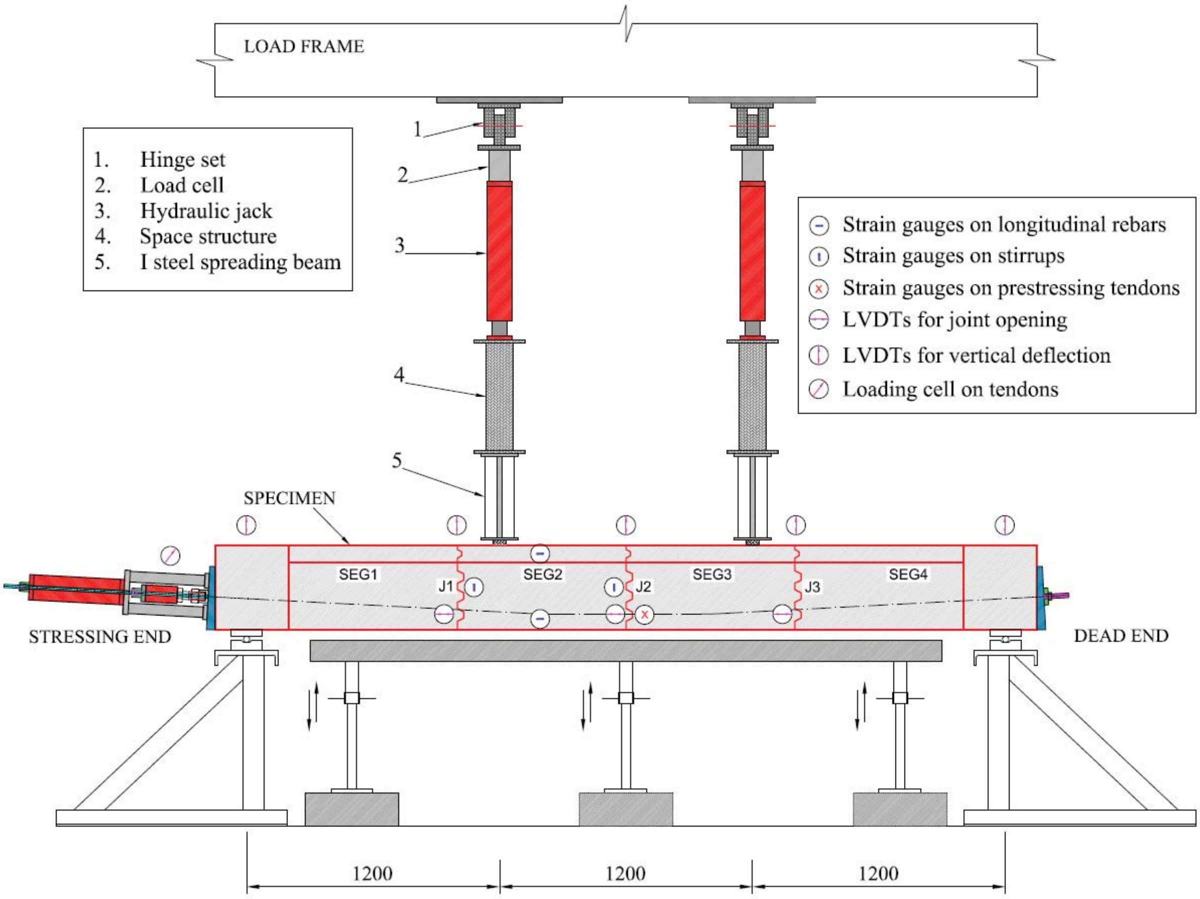

Fig. 6: Typical test set up

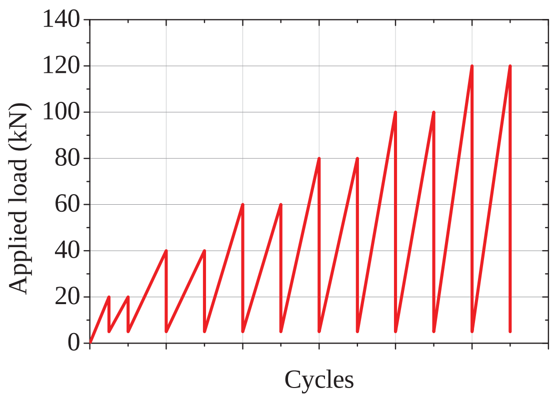

Fig. 7: Progressive loading cycles

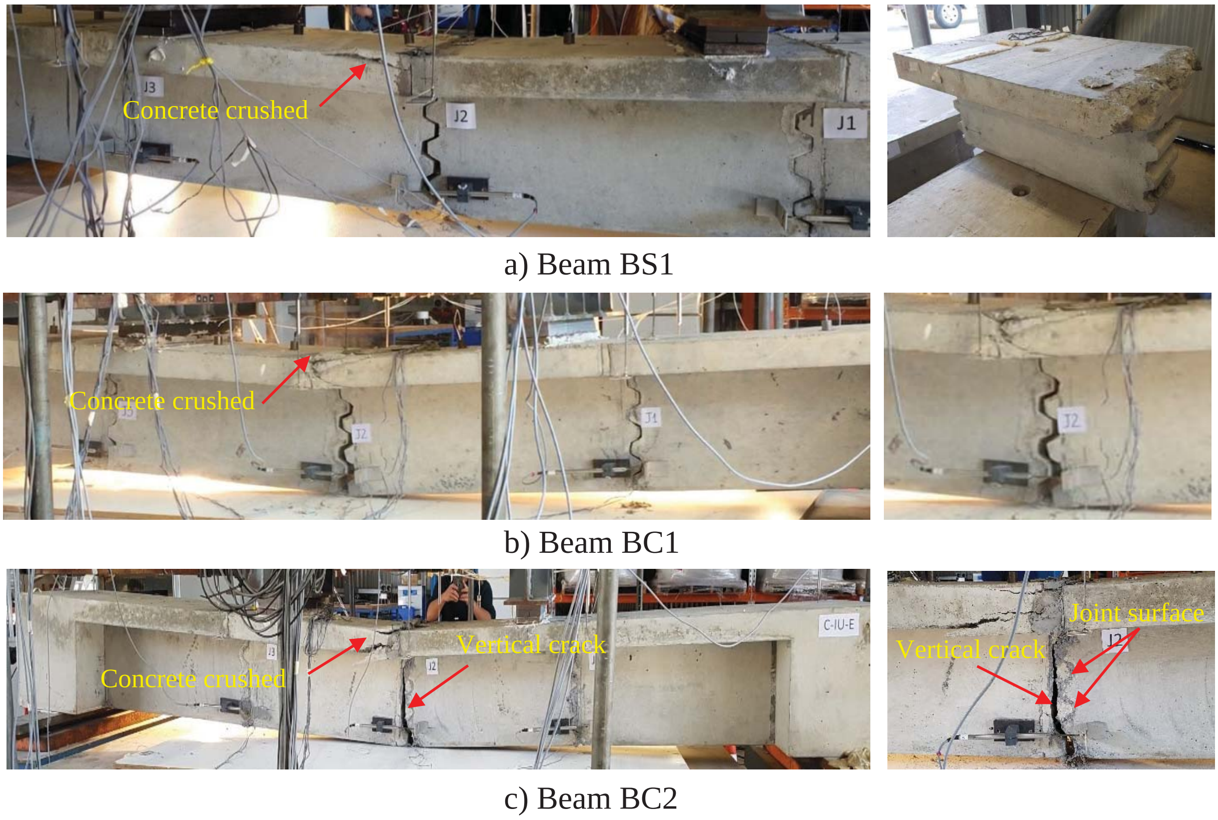

Fig. 8: Failure modes of the tested specimens

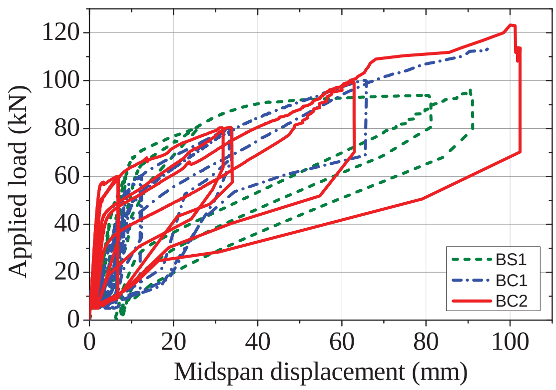

Fig. 9: Load vs deflection curves

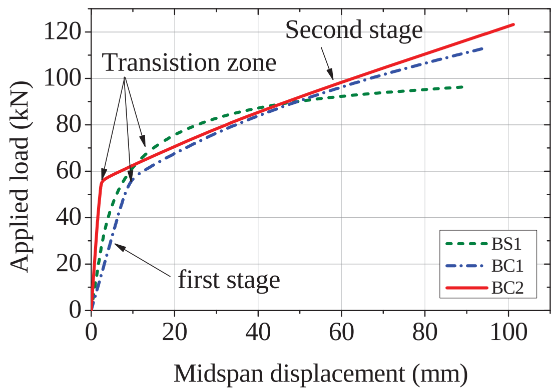

Fig. 10: Envelop curves of load vs deflection

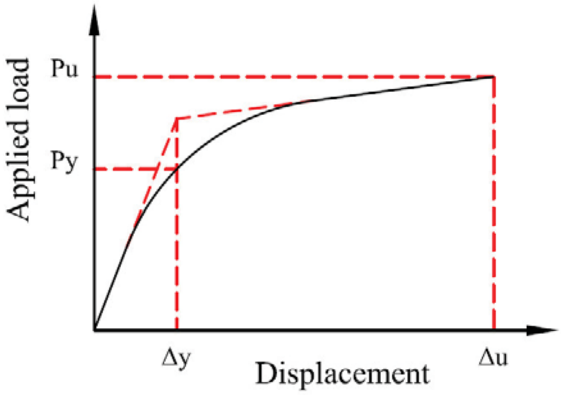

Fig. 11: Definition of yielding point

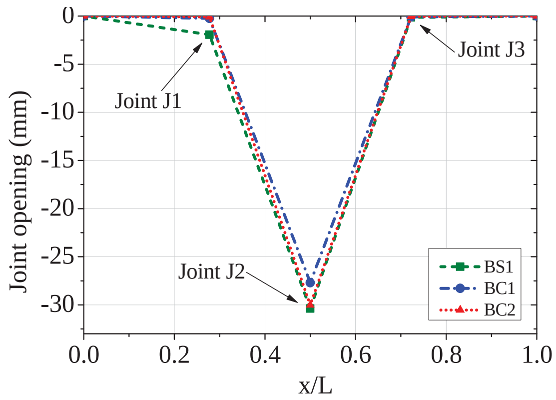

Fig. 12: Opening of joints along beam's axis

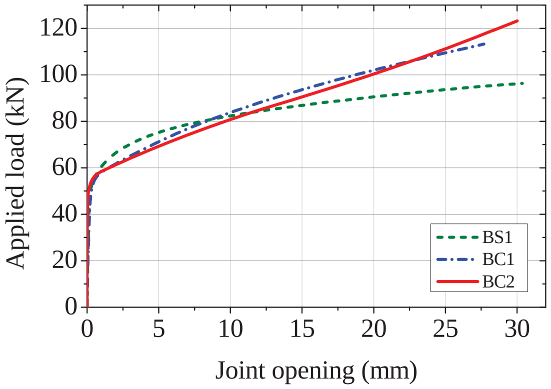

Fig. 13: Applied load vs opening of middle joint J2

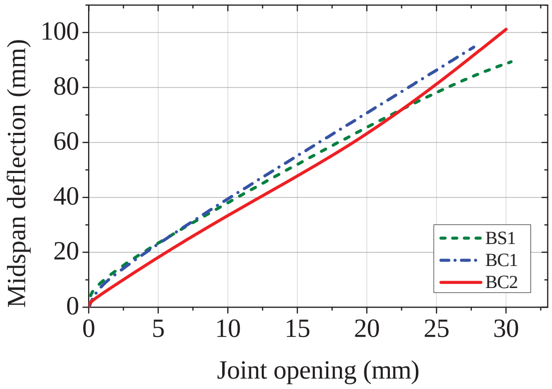

Fig. 14: Relationship between joint opening vs midspan deflection

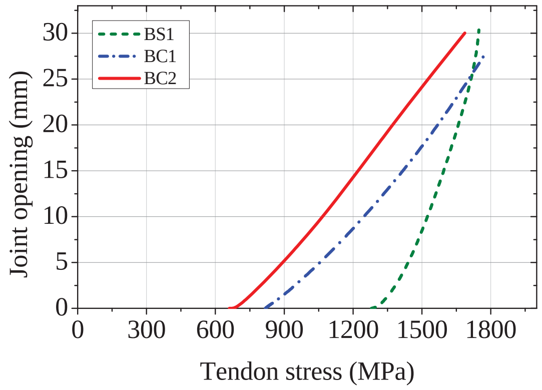

Fig. 15: Tendon stress vs joint opening

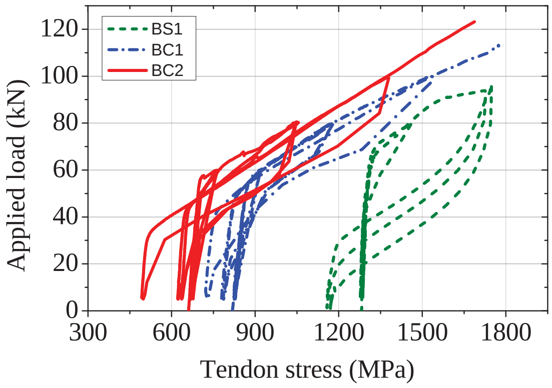

Fig. 16: Applied load vs tendon stress

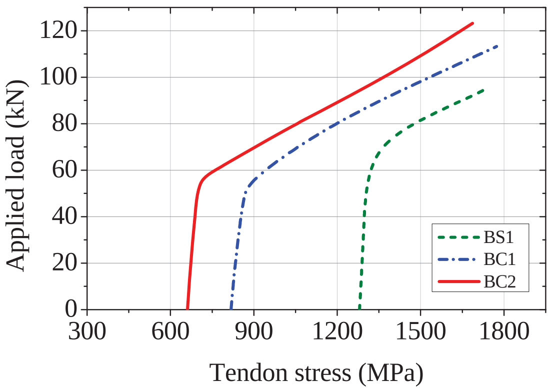

Fig. 17: Envelop curves of applied load vs tendon stress

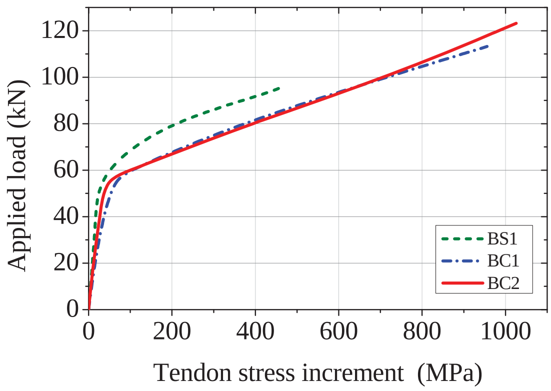

Fig. 18: Envelop curves of applied load vs tendon stress increment

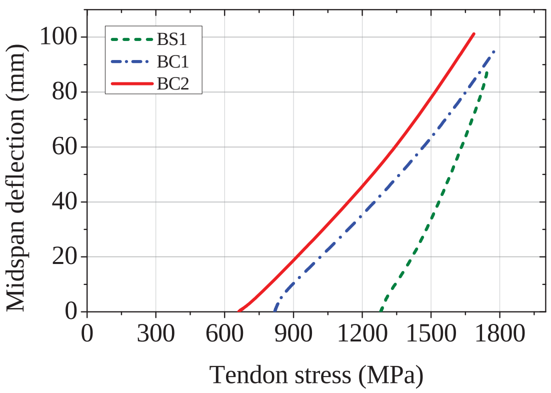

Fig. 19: Tendon stress vs midspan deflection

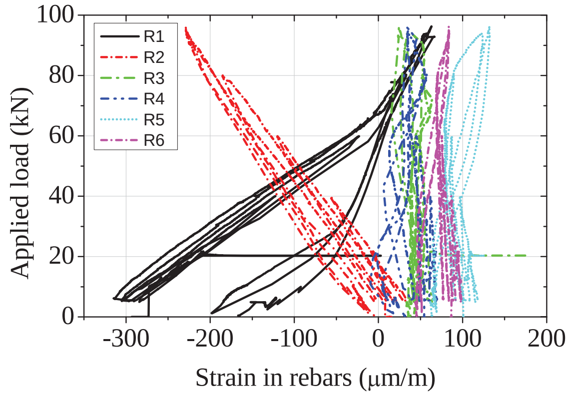

Fig. 20: Strain in rebars in Beam BS1

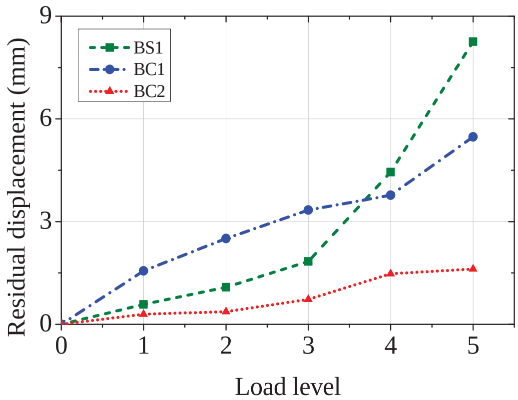

Fig. 21: Residual displacement of specimens

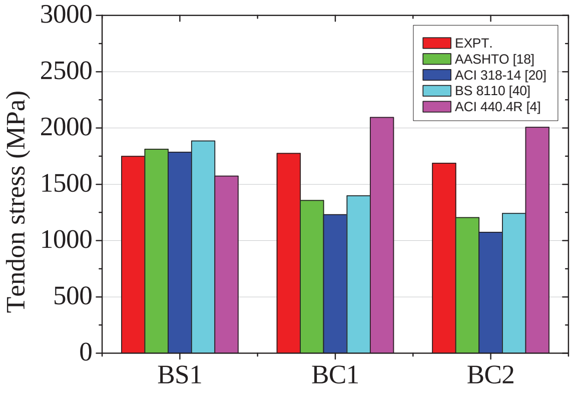

Fig. 22: Comparison of calculation of f_{ps}

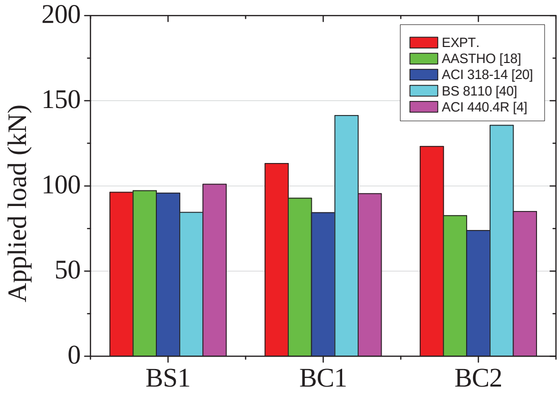

Fig. 23: Comparison of calculation of P_u

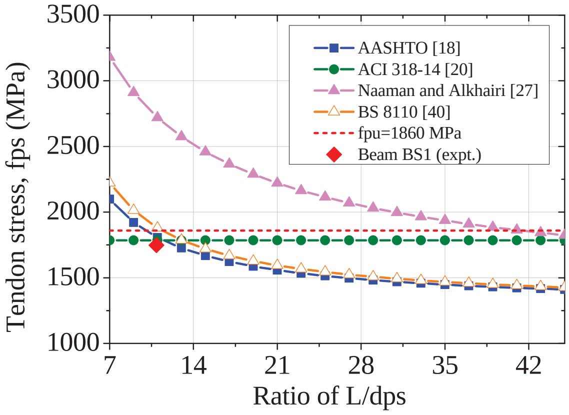

Fig. 24: Relationship between f_{ps} and L/d_{ps} ratio for beams with steel tendons

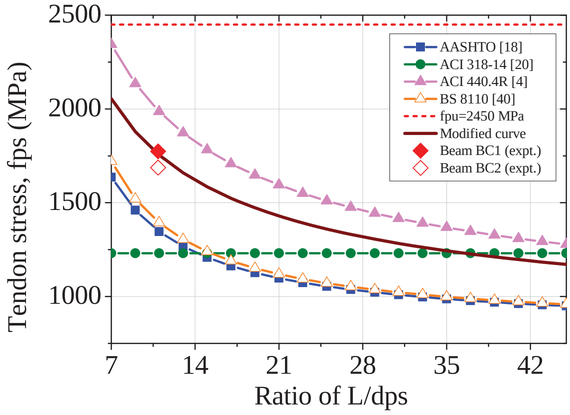

Fig. 25: Relationship between f_{ps} and L/d_{ps} ratio for beams with CFRP tendons

List of Tables

Table 1: Configuration of tested beams

Specimen	Tendon type	Joint type	Concrete strength	Effective tendon stress		Tendon force
			f_c' (MPa)	f_{pe} (MPa)	f_{pe}/f_{pu}	F_{pe} (kN)
BS1	2 steel tendons	Dry	44	1193	0.64	119
BC1	2 CFRP tendons	Dry	44	851	0.35	108
BC2	2 CFRP tendons	Epoxied	44	653	0.27	83

Table 2: Properties of materials

Type	Diameter (mm)	Area (mm^2)	Yield strength (MPa)	Ultimate strength (MPa)	Elastic modulus (GPa)
12-mm steel bars N12	12.0	113.0	534	587	200
10-mm steel bars N10	10.0	78.5	489	538	200
Steel tendon	12.7	100.0	1674	1860	195
CFRP tendon	12.9	126.7	N/A	2450	145

Table 3: Experimental testing results

Specimen	Applied load (kN)		Midspan deflection (mm)		Joint opening (mm)		Failure mode
	P_y	P_u	$\delta_{mid,y}$	$\delta_{mid,u}$	$\Delta_{J,y}$	$\Delta_{J,u}$	
BS1	51.2	96	5.4	89.4	0.20	30.44	Compression failure and yielding of tendons
BC1	53.4	113	8.4	94.7	0.55	27.70	Compression failure and rupture of CFRP tendons
BC2	54.1	123	2.3	101.1	0.07	30.02	Compression failure and rupture of CFRP tendons

Table 4: Ductility of the specimens

Specimen	Method 1			Method 2		
	Δ_y	Δ_u	Δ_u/Δ_y	A_y	A_u	A_u/A_y
BS1	5.4	89.4	16.6	201	7298	36.3
BC1	8.4	94.7	11.2	336	7853	23.4
BC2	2.3	101.1	44.0	67	9154	136.6

Table 5: Theoretical calculation of the four codes

Specimen	f_{pe} (MPa)	Δf_{ps} (MPa)			f_{ps} (MPa)				P_u (kN)		
		Theo.	Expt.	Theo/Expt	Theo.	Expt.	Theo/Expt	fexpt/fu	Theo.	Expt.	Theo/Expt
AASHTO [18]											
BS1	1280	531	468	1.13	1811	1748	1.04	0.94	97	96	1.01
BC1	818	539	956	0.56	1357	1774	0.76	0.72	93	113	0.82
BC2	661	543	1026	0.53	1204	1687	0.71	0.69	83	123	0.67
ACI 318-14 [20]											
BS1	1280	505	468	1.08	1785	1748	1.02	0.94	96	96	0.99
BC1	818	413	956	0.43	1231	1774	0.69	0.72	84	113	0.74
BC2	661	413	1026	0.40	1074	1687	0.64	0.69	74	123	0.60
ACI 440.4R [4]											
BS1	1280	294	468	0.63	1574	1748	0.90	0.94	84	96	0.88
BC1	818	1276	956	1.33	2094	1774	1.18	0.72	141	113	1.25
BC2	661	1345	1026	1.31	2006	1687	1.19	0.69	136	123	1.10
BS 8110 [40]											
BS1	1280	604	468	1.29	1884	1748	1.08	0.94	101	96	1.05
BC1	818	579	956	0.61	1397	1774	0.79	0.72	95	113	0.84
BC2	661	579	1026	0.56	1241	1687	0.74	0.69	85	123	0.69